

Advanced Applications of Viscous CFD for Hydrodynamic Design and Analysis of Twin-Skeg Ships

by

Nobuaki SAKAMOTO*, Yasutaka KAWANAMI*, Yasuo ICHINOSE**
and Shotaro UTO***

Abstract

As represented by the regulation of Energy Efficiency Design Index (EEDI), introduced by International Maritime Organization (IMO), maritime transportations are required to reduce their emissions of green house gases. To achieve this, it is crucial to design innovative hull forms with better hydrodynamic characteristics than existing ships. One of the candidates is a twin-skeg ship which is able to reduce emission of CO₂ evidenced by the fact that the Economical Index of twin-skeg container ship is approximately 20% smaller than conventional single-screw container ships. Based on these backgrounds National Maritime Research Institute (NMRI) designed 4,000TEU twin-skeg container ship with an electrical propulsion system supported by two off-centered podded propulsors. The off-centered podded propulsion system makes it possible to search its optimal location to minimize effective wake coefficient as well as to maximize hull efficiency. In proceeding such investigations for the twin-skeg container ship, an efficient approach is the complementary use of towing tank experiment and viscous computational fluid dynamics (CFD). Therefore the objective of the present study is to apply viscous CFD to carry out hydrodynamic design and analysis of the twin-skeg container ship. Six investigations are of the interest, e.g. 1) Ensure the accuracy of present viscous CFD method by quantifying the correlation in resistance and self propulsion coefficients between experiment and CFD, 2) Validation of local flow and predict optimal propeller location by CFD, 3) Hydrodynamic analysis of podded propulsor to be equipped on the present twin-skeg container ship, 4) Analysis of scale effect, 5) Parametric design of the skeg, and 6) Unit-based self propulsion analysis.

* Fluids Engineering and Hull Design Department、** EEDI Project Team、*** Ocean Engineering Department
原稿受付 平成26年7月31日
審査日 平成26年9月16日

Table of Contents

1. Introduction	2
2. Computational and experimental method	3
2.1 Overview of the computational method	3
2.2 Overview of the experimental method	3
3. Simulation design	4
3.1 Grid generation	4
3.2 Geometrical handling	5
4. Results and discussions	5
4.1 Correlation in resistance and self propulsion coefficients between experiment and CFD	5
4.2 Optimal propeller location and validation of local flow	7
4.3 Hydrodynamic analysis of podded propulsor to be equipped on MS791	9
4.4 Analysis of scale effect in local flow, 1-wt and POC	10
4.5 Effect of parametric change of the skag to resistance and self propulsion characteristics ..	12
4.6 Unit-based self propulsion analysis	13
5. Concluding remarks	16
References	17

1. Introduction

Twin-skeg ship is an innovative geometry to reduce emission of CO₂ evidenced by the fact that the Economical Index (E.I., required power per Twenty foot Equivalent Unit container) of twin-skeg container ship is approximately 20% smaller than conventional single-screw container ships (see Fig. 1)¹⁾, provided that their length between perpendiculars (L_{pp}) is equivalent to the container ship. The equipment of the skag is disadvantageous in comparison to single-screw ships in that 1) it is difficult to manufacture; 2) the building cost is higher since it requires two propulsors and relevant mechanical systems, and 3) the wetted surface area increases which results in larger frictional resistance. Yet the following advantages of twin-skeg ships must be emphasized, i.e. 1) redundancy in propulsors and mechanical systems contributes for navigational safety; 2) propeller loading of a twin-skeg ship is almost

half of a single-screw ship which can contribute to improve propeller open water efficiency η_o , thus compensating for the increase in frictional resistance, and 3) maneuverability of twin-skeg ship is generally considered to be better than single-screw ships (see for instance, Miyazaki et al. 2011)²⁾. Due to these advantages, National Maritime Research Institute (NMRI) has been investigating 4,000TEU twin-skeg container ship (termed MS791 hereafter) with an electrical propulsion system supported by two off-centered podded propulsors¹⁾³⁾. The off-centered podded propulsion system makes it possible to search its optimal location to minimize effective wake coefficient 1-wt as well as to maximize hull efficiency η_H . In order to carry out hydrodynamic design and analysis of MS791, viscous computational fluid dynamics (CFD) is definitely a powerful tool. The fundamental applications of viscous CFD for design and analysis of twin-skeg ships can be found in Lee et al. (2003a, 2003b)⁴⁾⁵⁾, Van et al. (2004a, 2004b)⁶⁾⁷⁾, Park and Chun (2009)⁸⁾, Kume and Hirata (2009, 2010)⁹⁾¹⁰⁾, Ochi and Nagaya (2010)¹¹⁾ and Kawabuchi et al. (2011)¹²⁾.

Followed by these results, the present study aims to achieve advanced application of viscous CFD for hydrodynamic design and analysis of MS791 which includes six investigations from I1 through I6, i.e.

- I1: Correlation in resistance and self propulsion coefficients between experiment and CFD
- I2: Validation of local flow and prediction of optimal propeller location by CFD
- I3: Hydrodynamic analysis of podded propulsor to be equipped on MS791
- I4: Analysis of scale effect in local flow, 1-wt and POC
- I5: Effect of parametric change of the skag to resistance and self propulsion characteristics
- I6: Unit-based self propulsion analysis

Among the above six investigations, I1, I2, I4 and I6 are most probably the first of their kind and none of the past studies⁴⁾⁻¹²⁾ have been

tried to carry them out.

The present study starts from I1 in order to obtain quantitative indications of the accuracy in the present computational methods. Once they are ensured, three investigations are made, e.g. 1) validations of local flow, 2) estimations of optimal propeller location, and 3) parametric design of the skeg. In the meantime the hydrodynamic characteristics of the podded propulsor to be equipped on MS791 are also investigated. Then, the hull and the podded propulsor are combined and their self propulsion characteristics are analyzed. Especially in local flow, 1-w_T and POC obtained through these studies, their computational analyses are extended to full scale.

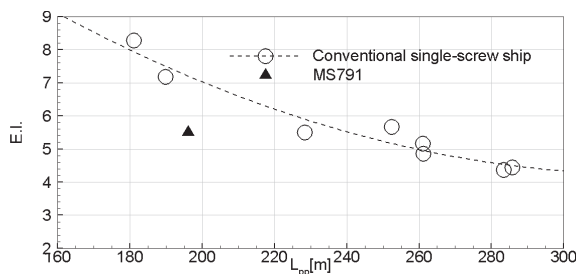


Fig. 1 Economical index (E.I.) for MS791¹⁾

2. Computational and experimental method

2.1 Overview of the computational method

All the simulations presented in this article are carried out by SURF ver.6.44, a finite-volume unstructured grid based Reynolds-averaged Navier-Stokes (RaNS) solver with Spalart-Allmaras (SA) one-equation turbulence model¹³⁾ and body-force propeller model¹⁴⁾ based on simplified propeller theory¹⁵⁾. Inviscid fluxes in momentum and turbulence transport equations are evaluated by the 2nd-order upwinding scheme based on the flux-difference splitting of Roe, and 1st-order upwinding scheme, respectively. Viscous fluxes appeared in momentum and turbulence transport equations are evaluated by the 2nd-order central differencing scheme. Temporal discretization is accomplished using 1st-order Euler backward differencing scheme with fully implicit manner. The code is parallelized by OpenMP®, and all the simulations presented in this article are

carried out by shared-memory type workstations. Readers can find more detailed description of the code in Hino et al. (2008)¹⁶⁾.

2.2 Overview of the experimental method

All the experimental data presented in this article are collected in the No.2 Towing Tank at NMRI which has the dimension of 400m in length, 18m in width and 8m in depth. Table 1 presents the major dimensions of MS791 and the propeller in full scale, and the model ship and the propeller are manufactured using these particulars with the scaling ratio 36.126. Figure 2 shows the stern view of the model ship equipped with a set of two pod casings, struts and propellers. The design speed of the ship is 20.0knots which corresponds to Froude number (Fn) based on L_{pp} equivalent to 0.235. The ship does not have any appendages but is fitted with bilge keels.

Six types of experiments are carried out, e.g. 1) resistance test with wake measurement utilizing bare hull with fitted bilge-keels; 2) propeller open water test (POT) without pod casing and its strut; 3) the POT with pod and its strut; 4) self-propulsion test with POT dynamometer for which the schematic figure of test configuration is shown in Fig. 3, 5) self-propulsion test with podded propulsors and attached dynamometers, and 6) cavitation test for podded propulsors attached to the hull. Test 1 measures total resistance R_{tm} , sinkage/trim and cartesian velocity components (u , v , w) at propeller plane. Tests 2 and 3 measure propeller open water characteristics (POC), e.g. torque Q , propeller thrust T_p or pod-unit thrust T_u as a function of advance velocity V_a , with/without pod casing and its strut. Test 4 measures only effective wake coefficient 1-w_T without pod casing and its strut. In order to calculate 1-w_T from the measured data, the POC from test 2 is leveraged. During test 4, the center of propeller traverses both in horizontal and vertical directions on the propeller plane in order to search the location where 1-w_T becomes minimum. Only port side is of the interest for this test due to the limitations in installing POT dynamometer onto the towing carriage. Notice that sinkage and trim are not

taken into consideration during the test. At the optimal location found in test 4, test 5 measures not only $1-w_T$ but also other self-propulsion coefficients, e.g. thrust deduction coefficient $1-t$ and relative rotative efficiency η_R with pod casings and struts. In order to measure self-propulsion coefficients, the POC from test 3 is leveraged. Different from test 4, podded propulsors are placed both side of the hull, and the model is free to be sunk and trimmed during the test. Test 6 utilizes Large Cavitation Tunnel at NMRI (test section has 8m in length, 2m in width and 0.88m in depth) to measure the fluctuation of pressure on the hull surface induced by rotating propeller and resultant cavitation for which the propeller locations are the same as test 5.

Table 1 Major dimension of MS791 and its propeller

Hull	
L_{pp} [m]	196.2
B [m]	42.809
d [m]	10.703
C_B	0.656
Propeller	
D_p [m]	8.2
Pitch ratio	1.02
EAR	0.35
Boss ratio	0.18
# of blades	3
Rotational direction	Right/Left
Wing section	NACA

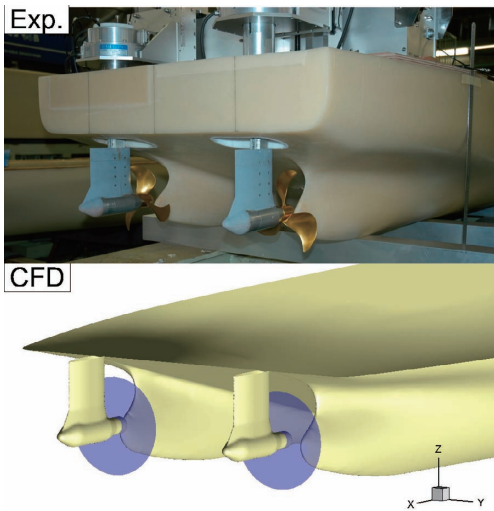


Fig. 2 Experimental (top) and computational (bottom) configurations of MS791

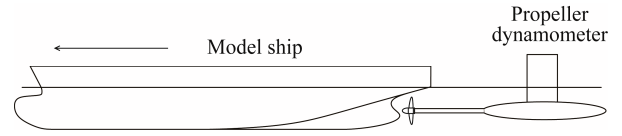


Fig. 3 Experimental configuration of self-propulsion tests with POT dynamometer

3. Simulation design

3.1 Grid generation

Two types of computational grids, i.e. structured and unstructured, are generated in the present study depending on target problems by the commercial grid generation package Gridgen®. In I1 through I5, the structured grid is prepared while unstructured grid is adopted for I6 since generation of structured grid is extremely challenging due to equipment of podded propulsor at the stern.

As an example of structured grid around bare hull, Figure 4a shows the overview of the computational domain in the hull vicinity. There are four blocks in one computational domain, i.e. bow block (Block 1), outer-skeg block (Block 2), inner-skeg block (Block 3) and free surface block (Block 4), and the total number of cells is approximately 1.3M (half side, medium grid). Figure 4b is the two dimensional perspective of the structured grid around podded propulsor for which total number of cells is approximately 5.0M (both sides, fine grid).

As an example of unstructured grid around a hull with podded propulsor Figure 4c shows the computational grid in the vicinities of stern. The grid has O-O type topology which consists of prism and tetrahedral cells. The total number of cells is approximately 7.2M (half-side ship with casing and strut, fine grid). Approximately 40 prism layers are extruded from the no slip surface in order to resolve boundary layer, and the rest of the computational space is filled up by tetrahedral cells.

For both structured and unstructured grids, the minimum spacing Δy normal to the hull surface is set in such a way that non-dimensional viscous length y^+ becomes less than 1 to ensure the fundamental accuracy of the present SA turbulence model. The

number of panel division for propeller disk is 5 and 36 in radial and circumferential directions, respectively.

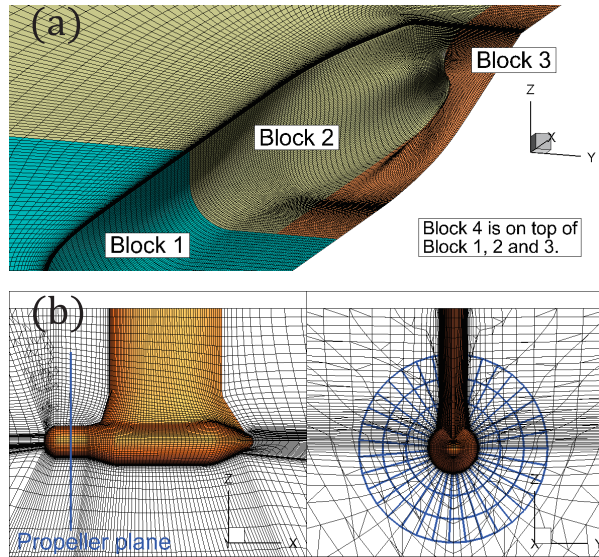


Fig. 4 Example of computational grid: (a) structured grid around bare hull, (b) structured grid around podded propulsor

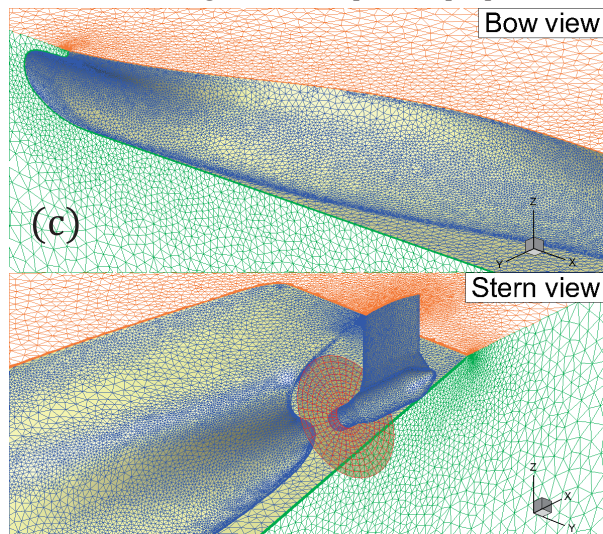


Fig. 4 Cont., (c) unstructured grid around hull with podded propulsor

3.2 Geometrical handling

Geometrical handling of the skeg is done by HullDes® which is a Computer Aided Design (CAD) and grid generation interface developed by collaborative works between ACT Co., Ltd. and NMRI. HullDes® defines hull surface via Non-Uniform Rational B-Spline (NURBS) and several pre-defined modification functions for hull surface have been prepared¹⁷⁾. These

features allow users to deform hull geometry as parametric as possible without missing the smoothness, i.e. the 2nd-order continuity, of hull surface. In I5, three design parameters have been investigated: 1) rake of skeg in yz-plane (termed vertical rake) from -20.0deg to +20.0deg, 2) rake of skeg in xy-plane (termed horizontal rake) from -1.8deg to 2.8deg, and 3) stern “UV” shape. Constraint condition for these deformations is that the displacement of modified hull is the same as the original hull, and it is accomplished throughout Lackenby’s criteria¹⁸⁾. Since these computational results are quite extensive, outcomes from horizontal rake are introduced in section 4.5. Figure 5 show the schematic definition for horizontal rake of skeg. The maximum displacement in y-direction is given to the longitudinal cusp of the skeg, and the waterlines within $0.70 \leq x/L_{pp} \leq 0.981$ and $-5.4545E-02 \leq z/L_{pp} \leq -1.8181E-02$ linearly move with the weight varying from 0.0 to 1.0 along $x/L_{pp}=0.7$ to 0.981. The angle of horizontal rake can be defined by the arc-tangent of the maximum displacement in y-direction at longitudinal cusp of the skeg divided by the distance between the root ($x/L_{pp}=0.7$) and longitudinal cusp ($x/L_{pp}=0.981$) of the skeg.

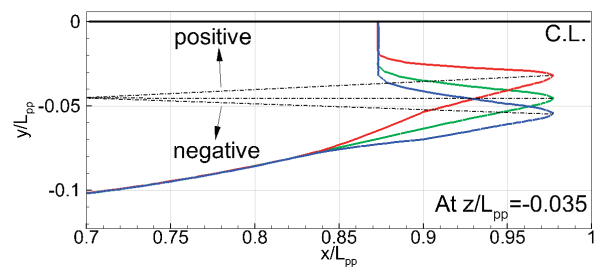


Fig. 5 Parametric change of the horizontal rake of the skeg

4. Results and discussions

4.1 Correlation in resistance and self propulsion coefficients between experiment and CFD

Figure 6 summarizes the correlations in resistance and self propulsion coefficients between experiment and CFD utilizing up to 13 hulls with twin-skeg¹⁹⁾. Four postulates for the present study are: 1) total number of cells

is up to 1.5M and 7.0M for structured and unstructured grid, respectively, 2) the computational result of form factor $1+k$ is determined by double-model simulation while Prohaska's method is used for the experimental result, 3) self propulsion point is set to ship point, and 4) all the ships are line-shaft type with the exception in MS791 series.

Overall results show that resistance (total resistance coefficient C_{tm} and $1+k$) and self propulsion coefficients are able to be estimated within 3% of the experimental data, with the exception in C_{tm} for "X series". The computational grid for "X series" is relatively coarse (0.8M, half side) compared to the others which fails to capture the wave making resistance coefficient C_w and yields large comparison error in C_{tm} . By these results it is confirmed that the present CFD solver and computational grids appropriately function to estimate resistance and self propulsion characteristics of different types of twin-skeg ships.

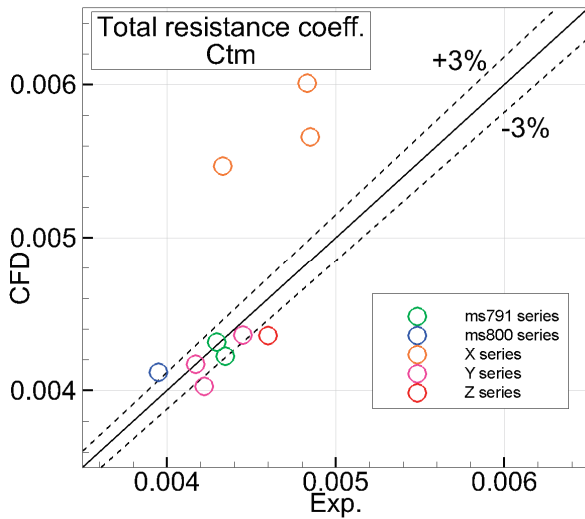


Fig. 6 Correlations in resistance and self propulsion coefficients between experiment and CFD

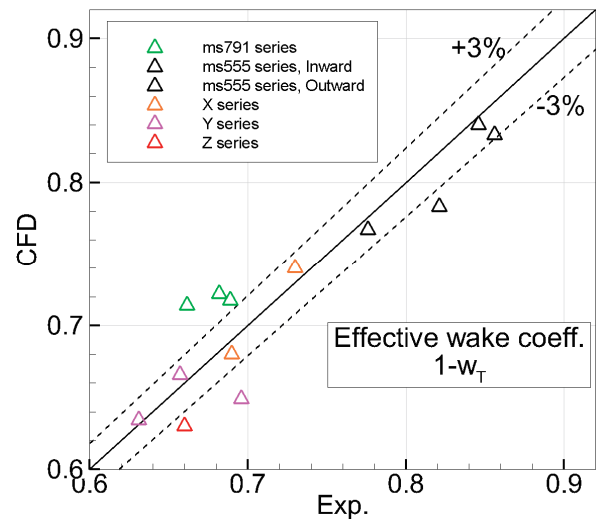
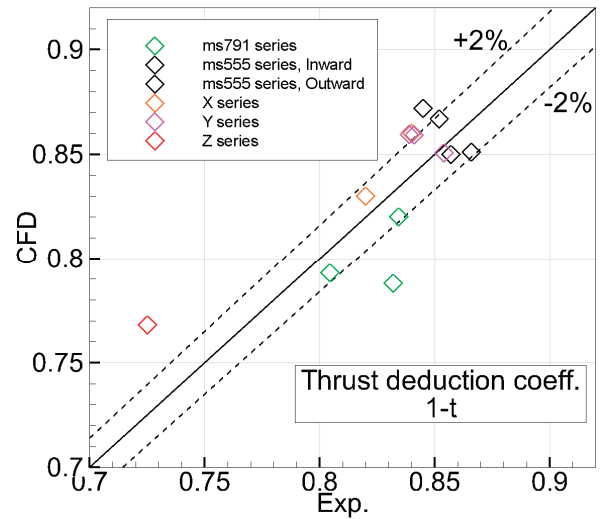
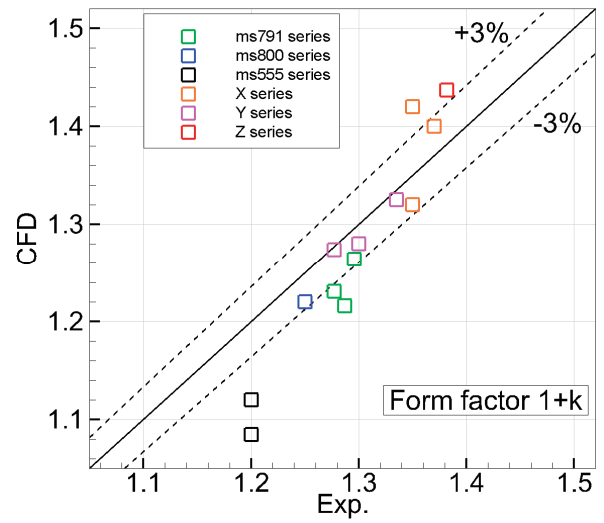


Fig. 6 Cont.

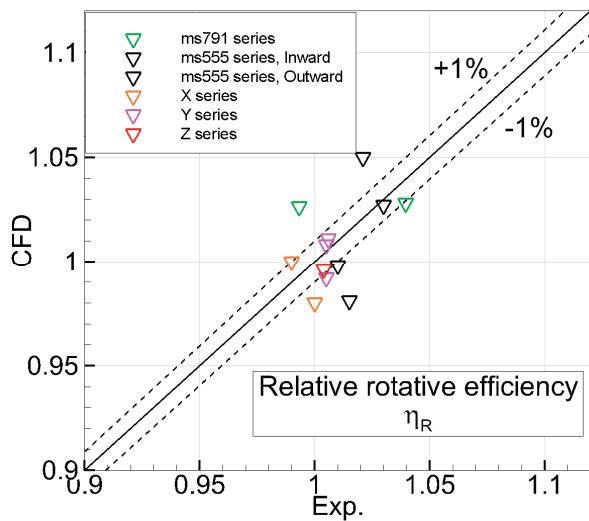


Fig. 6 Cont.

4.2 Optimal propeller location and validation of local flow

As the unique feature observed in the stern region of a twin-skeg ship, circulatory flow is generated by the skeg rotating from outside to inside of the skeg, in other words, the flow rotates counter clockwise observing from a stern. Assuming that the ship equips clockwise rotating propeller observing from a stern, there is likely to be an optimal propeller location where the circulatory flow generated by the skeg can be efficiently recovered by the propeller. Once the propeller is placed at its optimal location the apparent speed of propeller rotation increases. This yields decrease in advance coefficient J as well as in $1-w_T$, and increase in thrust coefficient K_T , which are the similar effect to contra-rotating propeller. Among most of the cases presented in this section, the F_n and the Reynolds number based on L_{pp} (R_n) are set to $(F_n, R_n)=(0.235, 7.48E+06)$.

Figure 7 summarizes the experimental and computational results of C_{tm} and C_w in different F_n . Figure 8 describes the eight locations of the propeller including experimentally identified¹⁾ optimal location (“*” in Fig. 8), and Fig. 9 shows the effect of propeller location to $1-w_T$. Notice that the case ID listed in Fig. 8 is in connection to what presented in Fig. 9. The present computation accurately predicts resistance quantities including the effect of free surface. At highest

$F_n(=0.3)$, C_{tm} and C_w are approximately 5% smaller than the experimental results which is most probably due to not taking the effect of trim and sink into consideration. The experimental results tend to provide smaller $1-w_T$ as the center of propeller approaches to the ship centerline as well as to the overhang part of the ship stern. Yet the locations aligned on $z/D_p=+0.1$ line (case4, case5 and case7) are not acceptable since the tip clearance of the propeller becomes too small which may results in undesirable vibration of the hull and noise induced by propeller cavitation. Therefore resultant optimal location found in the experiment is $(y/D_p, z/D_p)=(-0.1, +0.05)$. At the optimal location, maximum amplitude of pressure fluctuations measured in the experiment is 3.02 [kPa] in full scale, which is relatively low level for container ships navigating in 20.0knots in spite of the very narrow tip clearance ($15\%D_p$). The computational results estimate $1-w_T$ very well compared to the experimental data when the center of propeller locates at the center line of the skeg (case1, case2 and case5), optimal location (case Opt.) and at $y/D_p=0.1$ (case6). On the other hand, the results become larger than the experimental data when the center of propeller is close to the ship centerline (case3 and case4). As mentioned in Section 2.2, the experimental configuration utilizes only one POT dynamometer at port side of the ship, while the symmetric boundary condition is applied to xz -plane in the simulation. The effect of propeller interference in the computational configuration may yield such difference. The experimental study¹⁾ reproduces this effect where two podded propulsors are utilized to search the optimal location. When the center of propeller is outside of the skeg (case7), the result is smaller than the experimental data which is likely due to the lack of grid resolution.

In order to analyze the sources of the wake gain at optimal position, nominal wake coefficient $1-w_n$ and the circumferential mean velocity (CMV) along radial direction (r/R) at eight locations are calculated from the result of resistance simulation at $F_n=0.235$ as presented in Fig. 10. These two quantities are

the reasonable measures to quantify propeller inflow in axial and tangential directions, respectively. For $1-w_n$ at optimal location, it has approximately 4% to 6% smaller value compared to the other acceptable locations. For the CMV at optimal location, it has approximately 10% to 20% larger peak value compared to other acceptable locations.

Leveraging the optimal location, self-propulsion simulations are again performed in three different ship speeds as shown in Fig. 11. Overall trends show that the computational results reasonably follow the experimental results. The average comparison error in $1-w_T$ between the experimental and the computational results is approximately 2%. It is likely due to the error of estimation in J since the computational results of propeller-revolution per second (rps) agree very well to the experimental data²⁰. The discrepancy in $1-t$ is most likely due to the geometrical reason, i.e. the model ship used in the experiment has pod casing and its strut while the simulation does not. The discrepancy in η_R is conjectured to be the accuracy of torque coefficient K_Q in both open water and behind the ship.

Validations of local flow are carried out at the optimal propeller location. Figure 12 presents the computational and experimental result of the axial velocity distribution and cross-flow vectors at optimal propeller location. Figures 13a and 13b show the computational and experimental results of CMV along r/R and tangential velocity distribution along circumferential direction (θ) at $r/R=0.7$, respectively, on the propeller plane. For the axial velocity distribution, the computational result reproduces the bended contour of low-velocity region behind the skag very well compared to the experiment up to $u/U\sim 0.8$, although the $u/U\sim 0.9$ contour becomes diffusive inside and outside of the skag. The computational result of the cross flow vectors clearly shows the circulatory flow pattern rotating counter-clockwise observing from stern which is due to the upward velocity component enhanced by the tunnel buttock, and these phenomena agree quite well with what observed in the experiment. For the CMV

and tangential velocity distribution, both computational results generally agree well with the experimental data. Such information of stern flow field estimated by the present simulation recently utilized to design twisted rudder which contributes to improve propulsive performance of a certain twin-skeg ship¹⁹.

By these results it is confirmed that the present computational method appropriately functions to identify optimal propeller location owing to the accurate predictions in local flow characteristics. Readers can find more extensive results presented in this section in Sakamoto et al. (2013b)²⁰.

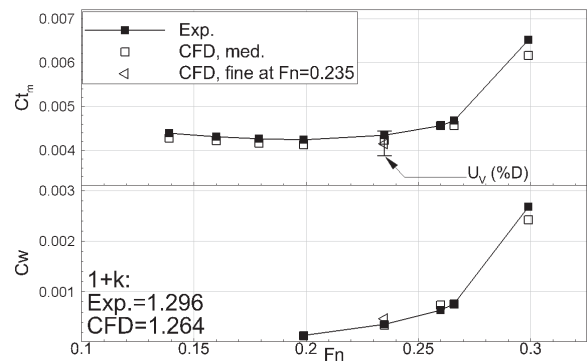


Fig. 7 C_{tm} and C_w for MS791, Exp. vs CFD

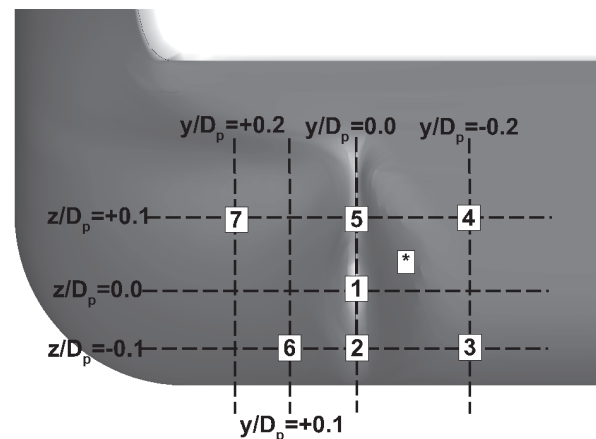


Fig. 8 Traversing location of propeller disk (port side, view from a stern)

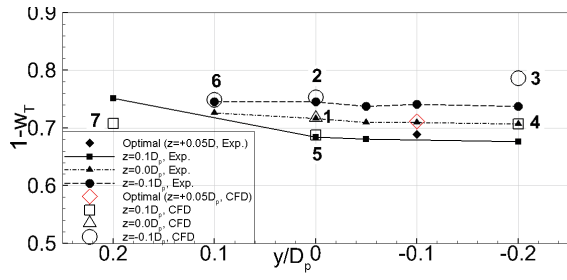


Fig. 9 Effect of propeller location to $1-w_T$ at $Fn=0.235$

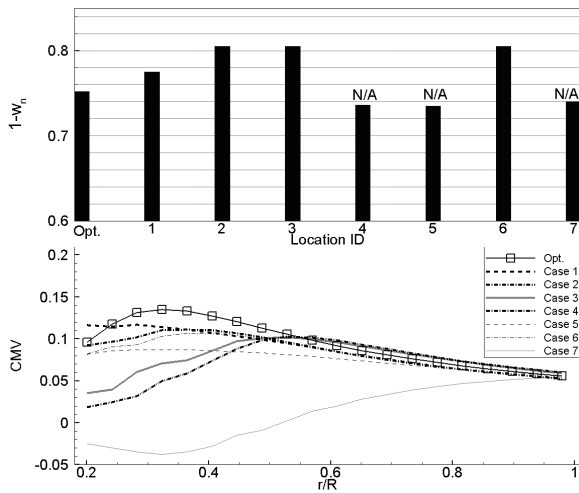


Fig. 10 Effect of propeller location to $1-w_n$ and CMV at $Fn=0.235$

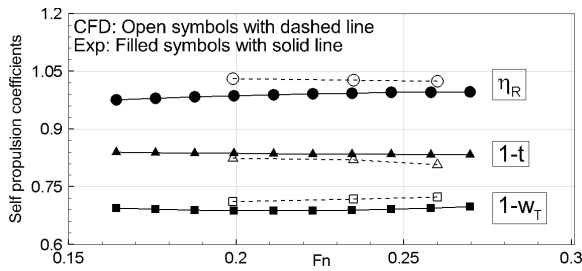


Fig. 11 Computational and experimental results of self propulsion coefficients at optimal propeller location

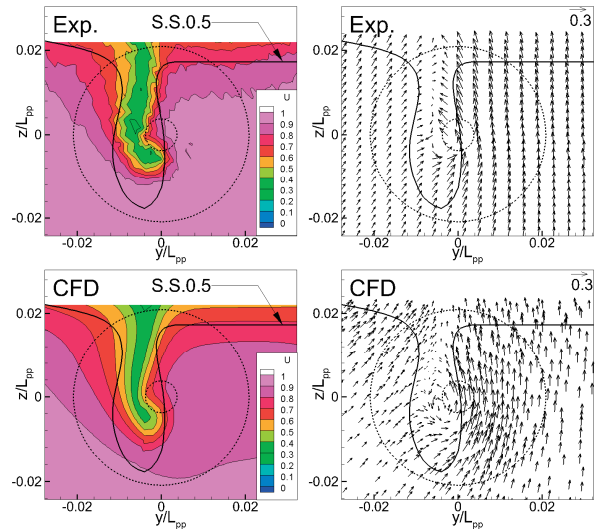


Fig. 12 Computational and experimental results of velocity distribution on the propeller plane at $Fn=0.235$

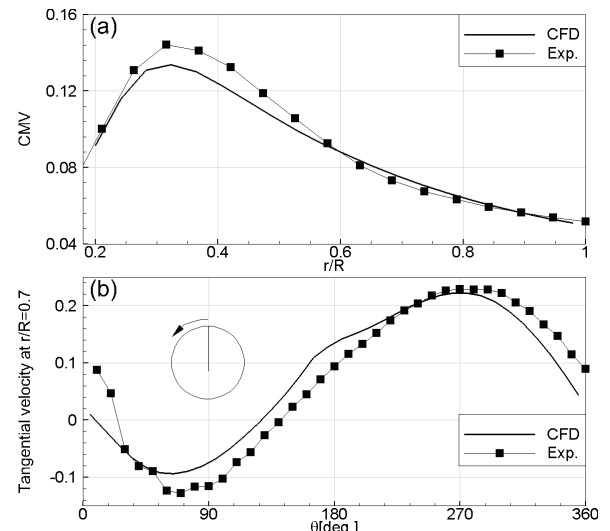


Fig. 13 Computational and experimental results of CMV and tangential velocity distribution on the propeller plane at $Fn=0.235$

4.3 Hydrodynamic analysis of podded propulsor to be equipped on MS791

Different from the previous sections, the podded propulsor is of the interest in this section. In order to carry out POT simulations of pod unit, the Reynolds number based on the chord length of the strut (RnC) is used, and it is $1.14E+05$ to $1.49E+05$ depending on J . Figure 14 shows the experimental and computational results of propeller-based and unit-based propeller open water characteristics (POC), respectively. Figure 15 describes

vortical structure around the podded propulsor identified by the 2nd-invariant of the rate of deformation tensor $Q=20$ iso surface. Current propeller model implemented in the CFD solver reproduces propeller-based POC in model scale very well. Unit-based POC in model scale estimated by the CFD agree well with the experimental data at three different J within the comparison effort E of 2.3% with respect to the experimental data which is most probably due to accurate estimation in resistance component acting on housing by CFD. As shown in Fig. 15 strong vortex is originated from the tail of the casing.

By these results it is confirmed that the present computational method appropriately functions to estimate POC of podded propulsor as well as vortical structure around housing. Readers can find more extensive results presented in this section in Sakamoto et al. (2013c)²¹.

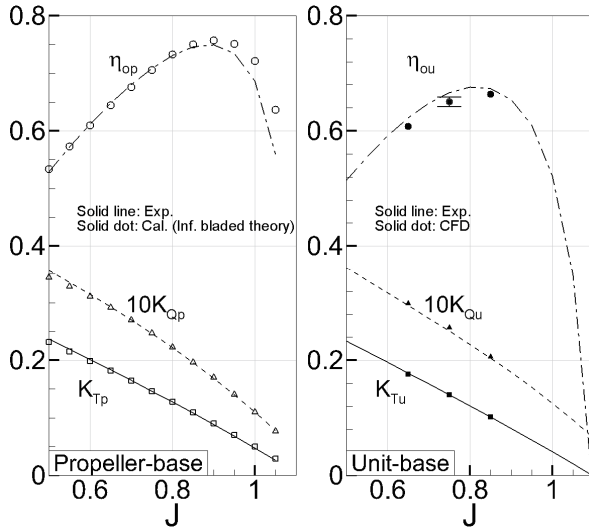


Fig. 14 POCs obtained by propeller base and unit-base analyses in model scale

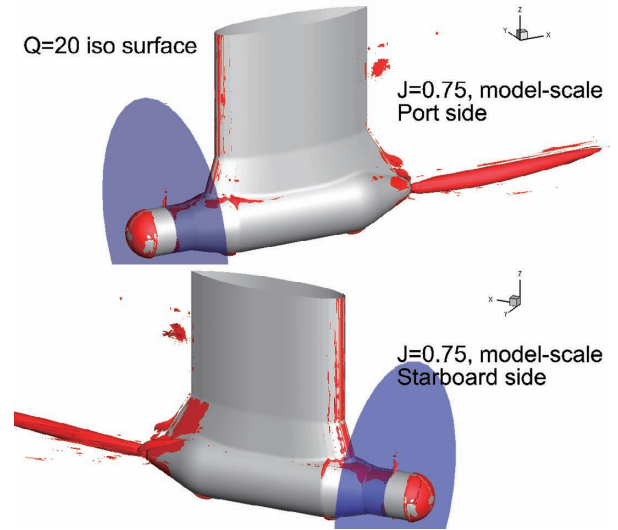


Fig. 15 Vortical structure around podded propulsor in model scale

4.4 Analysis of scale effect in local flow, 1-wr and POC

The scale effect has been one of the important issues which remain to be clarified in the ship hydrodynamics. In this section, investigations are made to understand scale effect in MS791 and its podded propulsor, especially in local flow, 1-wr and POC of pod unit using full scale CFD simulation. Among all the simulations presented in this section, the effect of free surface is neglected and thus the Rn is $7.48E+06$ and $1.70E+09$ in model and full scale, respectively, for MS791 and RnC is up to $1.49E+05$ and $3.40E+07$ in model and full scale, respectively, for the podded propulsor. The total number of cells for the computational grid is approximately 9.1M and 5.0M for MS791 and podded propulsor, respectively. For consistent comparison between model and full scale, the computational grids for full scale are utilized to perform model scale simulations.

Figure 16 shows the scale effect on the axial velocity and cross flow vector together with turbulent eddy viscosity around propeller plane. The scale effect on the turbulent eddy viscosity is significant inside the skeg tunnel especially close to the hull and upper outside of the skeg tunnel. The axial velocity profile shrinks in conjunction with the distribution of turbulent eddy viscosity. In cross-flow vector, the scale effect is likely to become most significant at $(y/L_{pp}, z/L_{pp}) \sim (0.044, -0.025)$.

Figure 17 presents the CMV distribution along radial direction in model and full scale on the propeller plane. The CMV in full scale totally shifts upward compared to the model scale while its peak location remains the same at $r/R \sim 0.32$. By these results, the scale effect is apparent not only in the axial velocity but also in the circumferential velocity which should be considered in the existing scaling criteria of $1-w_T$, for instance, ITTC1978 method²²⁾ for more realistic extrapolation. Figure 18 shows $1-w_T$ in full-scale obtained by three different scaling criteria, e.g. full-scale CFD simulation, Yazaki's method (half-breadth used) and ITTC 1978 method without rudder effect. The numbers above the bar-chart describe the difference between full-scale computational result and scaled computational and experimental results. The current results show that the two existing methods provide reasonably scaled results in both computational and experimental results in comparison to the full-scale CFD result. Although Yazaki's method is originated from the correlation between main particulars (Breadth/Draught) of single-screw ships, their model-scale and full-scale effective wake fractions, it provides realistic results in MS791. Figure 19 is the same as Fig. 15 but obtained from full scale CFD simulation. Strong vortex is originated from the tail of the casing which is common in model (see Fig. 15) and full scale while the vortices behind the strut are apparent in full scale than in model scale. One idea to improve the geometrical design of the current casing is to modify the shape of its trailing edge which will contribute to recover the rotational energy. This could decrease resistance of housing for both model and full scale and thus resultant pod unit thrust coefficient K_{Tu} and pod unit open water efficiency η_{ou} could be improved. In full scale it is common for both RANS method and ITTC method that the difference between model and full scale (Δ) of K_{Tu} and η_{ou} become larger with the increasing J as quantified in Table 2. The Δ by ITTC method are generally smaller than those of RANS method, and this difference is conjectured to be caused by the scaling of resistance acting on housing. Readers can find

more extensive results presented in this section in Sakamoto et al. (2011)²³⁾ and Sakamoto et al. (2013c)²¹⁾.

Table 2 Estimated changes in K_{Tu} and η_{ou}

J	Δ of K_{Tu} (%Model)		Δ of η_{ou} (%Model)	
	ITTC	RANS	ITTC	RANS
0.65	+1.17%	+2.91%	+1.17%	+3.60%
0.75	+1.62%	+4.70%	+1.62%	+4.65%
0.85	+2.45%	+7.67%	+2.45%	+6.94%

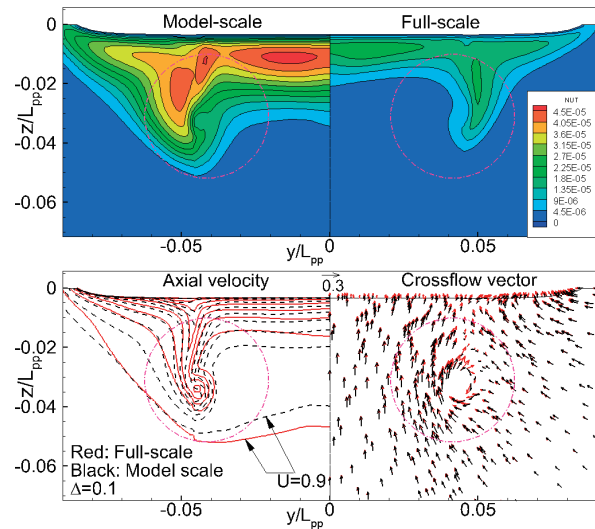


Fig. 16 Scale effect in turbulent eddy viscosity (top) and velocity distributions (bottom)

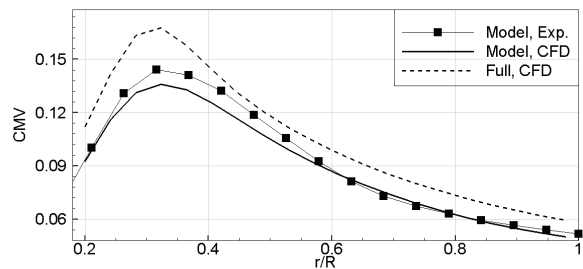


Fig. 17 Scale effect in CMV on the propeller plane

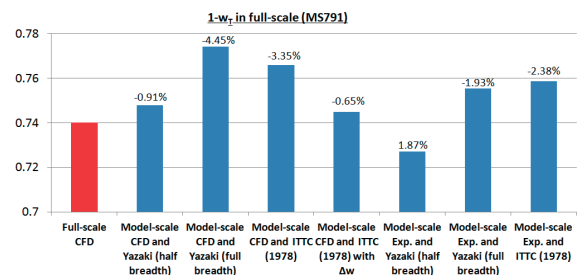


Fig. 18 $1-w_T$ in full scale obtained by different extrapolation criteria

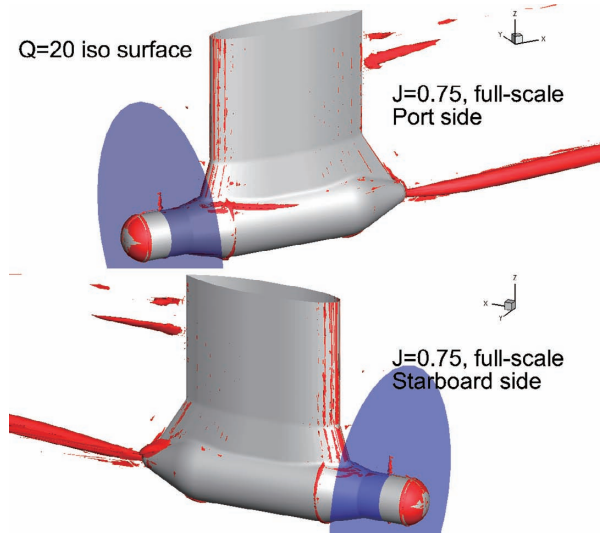


Fig. 19 Vortical structure around podded propulsor in full scale

4.5 Effect of parametric change of the skeg to resistance and self propulsion characteristics

In terms of hull design, podded propulsors make skegs free from propeller shaft which means that their geometrical design would be much more flexible than those of conventional twin-skeg ships. In order to take this advantage, understanding relationship between skeg geometry and resistance/self propulsion/local flow characteristics of the ship would be quite important for better design of a hull. In this section, the original geometry is MS791 and the results of “horizontal rake angle” are presented, and the rest of the results (vertical rake/stern UV variations) can be found in Sakamoto et al. (2012)²⁴. In all the results presented in this section, the F_n and the R_n are set to $(F_n, R_n) = (0.0, 7.48E+06)$. In order to estimate delivered power P_D , the C_w at $F_n = 0.235$ is taken from Sakamoto et al. (2013b)²⁰. Notice that the P_D is “tank” P_D and thus the extrapolations in $1-w_r$ and η_o to full scale are not taken into consideration.

Figure 20 summarizes the computational results of resistance and self-propulsion coefficients as well as estimated P_D depending on the variation of horizontal rake. All the physical quantities change in accordance with linear or quadratic polynomial. Maximum horizontal rake in positive direction minimizes C_{tm} by 3.6%original, yet the variation of horizontal rake has relatively minor influence

on η_D by 1.0%original. This trend results in P_D minimized by 1.4%original at largest horizontal rake in positive direction. As shown in Fig. 20, the trend of $1-w_n$ is opposite to $1-w_r$ which is most likely due to the increase of CMV along radial direction up to 1.5 times stronger than original as the horizontal rake becomes larger in negative direction, see Fig. 21. Figure 22 shows the computational results of pressure distribution on the hull for original and positive-maximum horizontal rake. As the horizontal rake becomes larger in positive direction, the low pressure region inside the tunnel stern becomes smaller and it slightly becomes larger at outside the tunnel stern. This phenomenon can be explained by assuming the skeg as an airfoil with attack angle (leading edge is $x/L_{pp} = 0.7$ and trailing edge is a longitudinal cusp of the skeg). Positive horizontal rake makes outside skeg suction side, and inside the skeg pressure side, which contributes to decrease pressure resistance inside the skeg and $1+k$ can be minimized by 3.5%original.

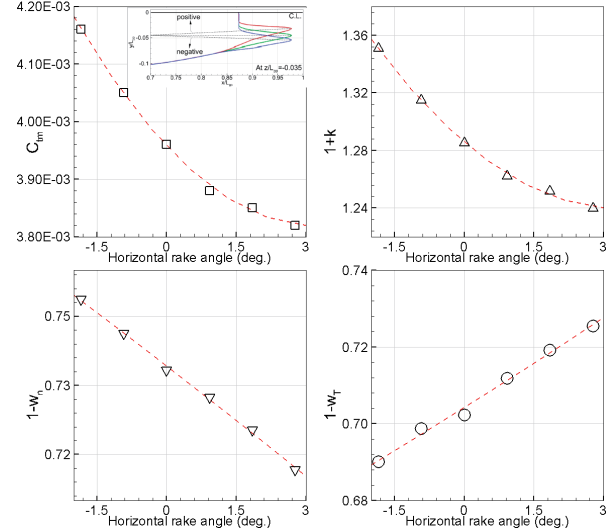


Fig. 20 Computational trend of resistance and self propulsion coefficients in the variation of horizontal rake

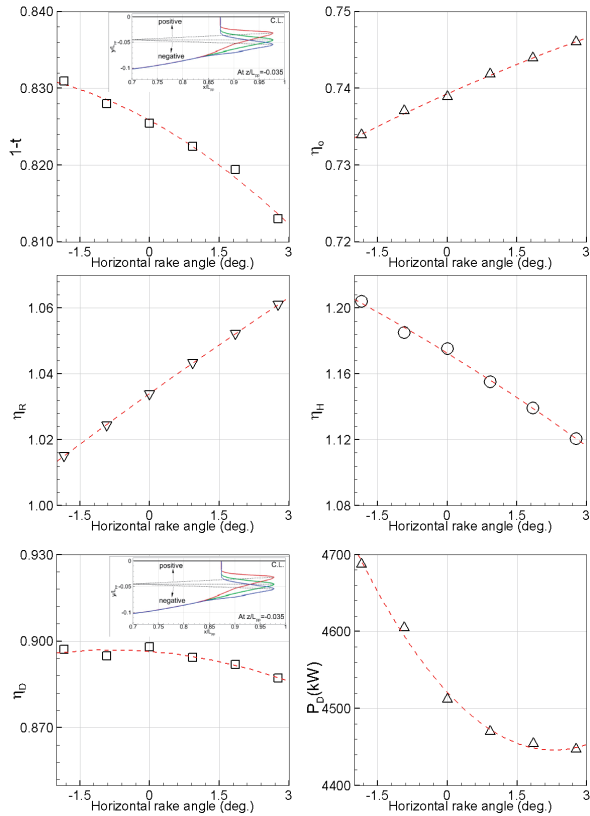


Fig. 20 Cont.

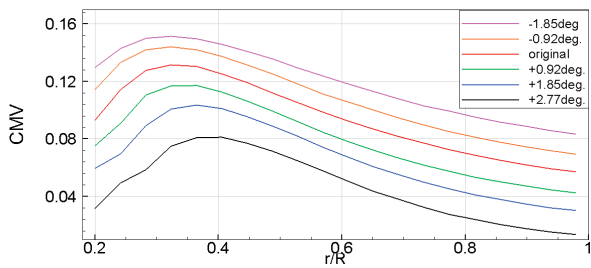


Fig. 21 Computational trend of CMV on the propeller plane in the variation of horizontal rake

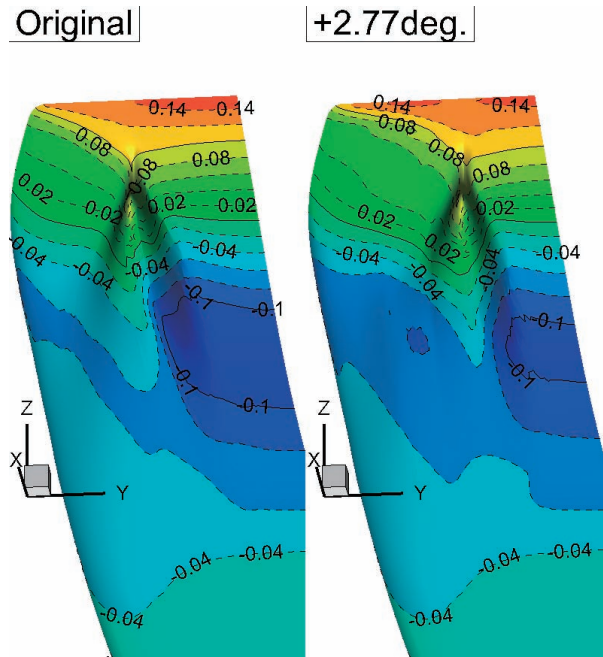


Fig. 22 Difference of pressure distribution around the yunnel buttock, original (left) vs optimal (right)

4.6 Unit-based self propulsion analysis

Two different approaches have been known as self propulsion analyses for ships equipped with podded propulsors. Figure 23 describes the difference of the two analyses²⁵⁾, i.e. the propeller-based analysis (PBA) and the unit-based analysis (UBA). For the PBA, the propeller is isolated from the housing so that the housing is considered as a part of a ship hull. The analysis consists of propeller open water test (POT) with isolated propeller and resistance/self propulsion tests with a ship hull and housing. For the UBA, the housing is considered as a part of propeller (termed “pod unit” hereafter), and thus it is isolated from a ship hull. In such cases, the POT is carried out using pod unit, the resistance test is conducted with a bare hull, and a ship hull with pod unit (termed “appended” hereafter) is leveraged to perform self propulsion test. The PBA is superior to its simplicity while the UBA is able to reproduce more “realistic” condition since the propeller open water characteristics (POC) for podded propulsor is usually provided as pod unit. Ukon and Fujisawa (2004)²⁶⁾ quantified the effect of these analyses to self propulsion coefficients by towing tank experiment, but

few computational studies have been found so far. Once the viscous CFD is applicable for the UBA, it would be beneficial for designers to save costs for experiments as well as to obtain detailed flow information around a pod unit and an appended hull.

The UBA utilizing whole CFD results, i.e. POT, resistance and self propulsion simulations, goes through the following procedure associated with Table 3 and Fig. 24.

1. Compute form factor $1+k$ from #2 and then perform #3 for each ship speed. The non-dimensional propeller rotation speed (rev) is automatically detected by the code, and set this rev as n_0 .
2. Set $n_1=0.9n_0$ and $n_2=1.1n_0$, and then use them to perform two additional self propulsion simulations with constant revs.
3. Define following parameters:
 - R_{bare} : Total resistance coefficient of bare hull from #2
 - R_{tot} : Total resistance coefficient of appended hull from #3
 - R_{pod} : Housing resistance coefficient from #3
 - R_{sp} : Hull resistance coefficient from #3
(= $R_{tot}-R_{pod}$)
 - n_u : rev at self propulsion point in the UBA
 - T_n : Net propeller thrust (non-dimensional) from #3
 - T_u : Non-dimensional unit thrust from #3
(= $T_n \cdot R_{pod}$)
 - SFC_w : $=(1+k)(C_{f0m}-C_{f0s})-\Delta C_f-C_w$ from #2 and Exp.

where C_{f0m} and C_{f0s} are model and ship frictional resistance coefficients from Schoenherr's formula, ΔC_f is the model ship correlation allowance ($=2.0 \times 10^{-4}$ in the present study).

then, draw graphs of rev vs $R_{sp}-SFC_w$, and rev vs T_u via linear regression line (see Fig. 24a). The cross point of the two lines represents the "self propulsion point" in the UBA. The cross point provides n_u and T_u , so the thrust coefficient in the unit-base analysis KT_u is obtained.
4. Obtain torque coefficient KQ from step 1 and step 2, then draw a graph of rev vs KQ via 2nd-order polynomial interpolation (see Fig. 24b). Find KQ at n_u obtained in step 3, and then it becomes KQ behind the hull.
5. Prepare the unit-based POC from #1, and then follow standard thrust identity method using

KT_u obtained at step 3 to calculate effective wake coefficient $1-w_T$ and KQ at open water (see Fig. 24c). The unit-based propeller open water efficiency η_{ou} is also calculated from KT_u , advanced coefficient J and KQ (open water).

6. Calculate relative rotative efficiency η_R using KQ (behind the hull) and KQ (open water) obtained at step 4 and step 5, respectively.
7. Use R_{bare} , SFC_w and T_u to calculate thrust deduction coefficient $1-t$ in the UBA, i.e. $1-t = (R_{bare}-SFC_w)/T_u$

The computational result of $1+k$ of the bare hull is 1.212 while it is 1.218 for the appended hull which indicates that the effect of housing is almost negligible for the present geometry. The same trend is reported by Ukon and Fujisawa (2004)²⁶. Figure 25 summarizes the experimental and computational results of self propulsion coefficients. The computational results generally show nice agreement to the experimental data. Considering the application of the present analysis to practical use, following suggestions can be made; 1) the PBA is easy to perform and thus it is suitable for "series" CFD calculations among different hull/housing geometries and relative comparison of their propulsive performance, 2) when the hydrodynamic performance of the pod unit and bare hull are to be investigated individually, the UBA is suitable method for such configuration and is feasible using full CFD simulations. Figure 26 describe the computational results of the effective wake distribution with cross flow vectors on the propeller plane with/without housing. The effective wake is defined based on the assumption²⁷ that the total wake (or total velocity) is decomposed into the following components as

$$\begin{aligned} [\text{total vel.}] &= [\text{effective vel.}] + [\text{induced vel.}] \\ &= [\text{nominal vel.}] + [\text{interaction vel.}] + [\text{induced vel.}] \end{aligned} \quad (1)$$

According to Eq. (1), the effective wake field is calculated by subtracting the propeller induced velocity which is obtained by the propeller model from total velocity at self propulsion point. The effective wake field with housing shows slower effective velocity region at six and twelve o'clock direction than that of without housing. Since the difference in the

nominal wake field is localized only at six o'clock direction (not shown in the present article), it is conjectured that the difference in the effective wake is due to the interaction between the propeller and the housing. This is one of the reasons that the averaging of the effective wake over the entire propeller plane is 0.74 for the case with housing while it is 0.76 for the case without housing. Figure 27 shows the streamline and pressure distribution in the vicinity of the ship stern with/without propeller. Notice that the streamline is colored by the non-dimensional axial velocity. When the propeller is not turned on, the streamlines behind the housing rotate counterclockwise observing from the stern. Once the propeller starts working, clockwise rotating propeller recovers the counterclockwise circulatory flow originated from the skeg. It also accelerates the flow in the axial direction which results in the changing in the pressure distribution on the housing. Readers can find more extensive results presented in this section in Sakamoto et al. (2013d)²⁸⁾.

Table 3 Necessary CFD simulations for unit-based self propulsion analysis

#	Vs (knot)	Rn (x10 ⁶)*	Type	Config.
1	-	0.11, 0.13, 0.15	POT	Pod-unit
2	16.9	6.35	Resist.	Bare
3	20.0 22.6	7.48 9.55	Self prop.	Appended

*: based on strut chord length for POT, based on Lpp for resist. And self prop.

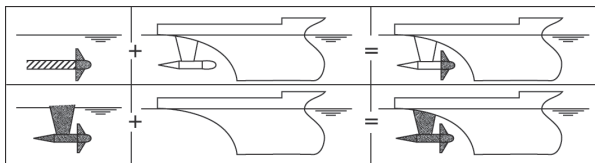


Fig. 23 Schematic figure of propeller-based (top) and unit-based (bottom) self propulsion analysis²⁵⁾

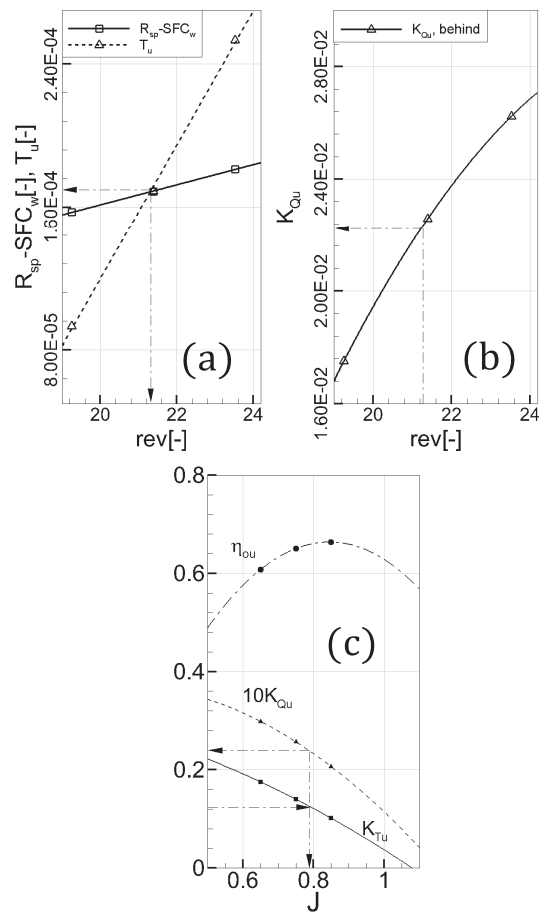


Fig. 24 Computational procedures of unit-based self propulsion analysis

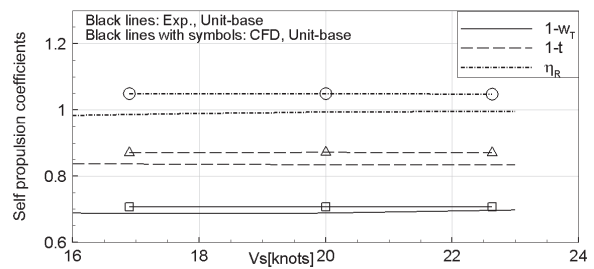


Fig. 25 Computational and experimental results of self propulsion coefficients obtained by unit-based analysis

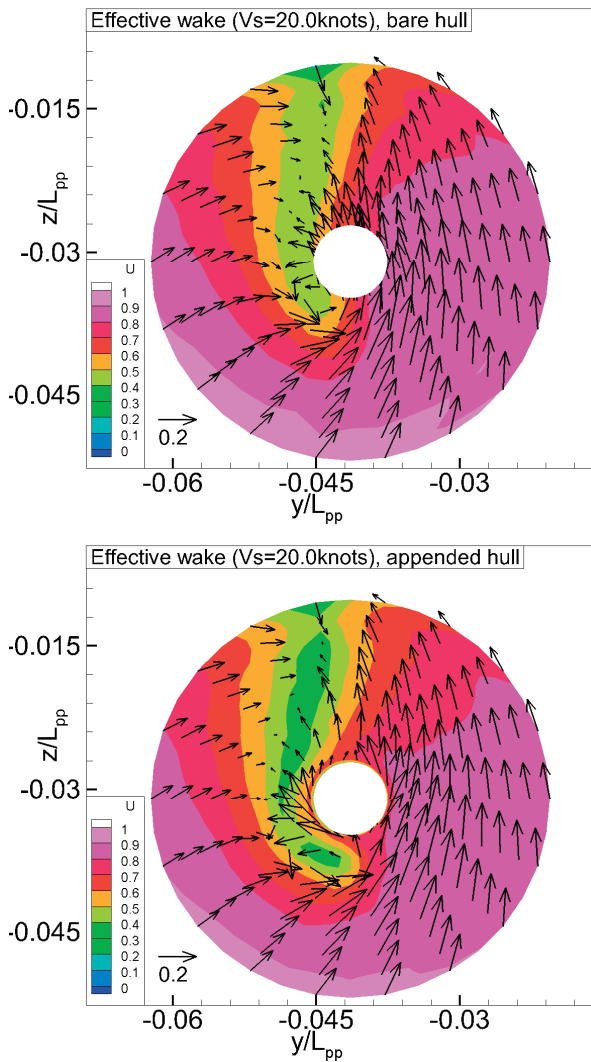


Fig. 26 Computational results of effective wake field at propeller plane without (top) and with (bottom) podded propulsor

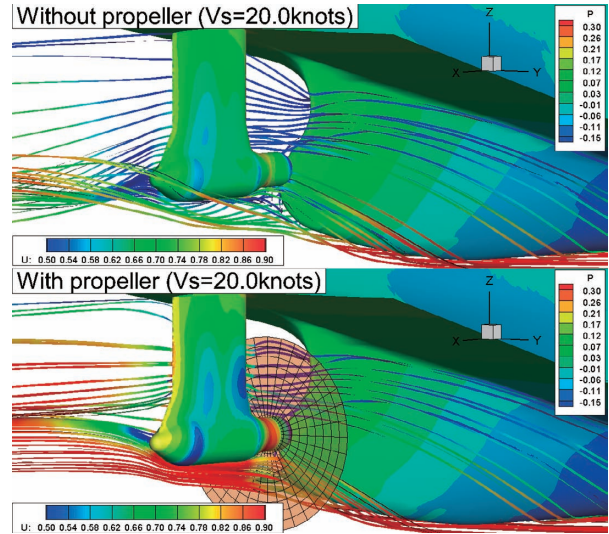


Fig. 27 Computational results of streamline and pressure distribution in the stern vicinity without (top) and with (bottom) propeller

5. Concluding remarks

Viscous CFD simulations are carried out in order to perform hydrodynamic design and analysis of MS791 - 4,000 TEU twin-skeg container ship with podded propulsor. In-house viscous CFD solver SURF ver6.44 is utilized for the present study. Six investigations are of the interest, i.e.

- I1: Correlation in resistance and self propulsion coefficients between experiment and CFD
- I2: Validation of local flow and prediction of optimal propeller location by CFD
- I3: Hydrodynamic analysis of podded propulsor to be equipped on MS791
- I4: Analysis of scale effect in local flow, 1-wr and POC
- I5: Effect of parametric change of the skeg to resistance and self propulsion characteristics
- I6: Unit-based self propulsion analysis

From I1 the correlations in resistance and self propulsion coefficients between experiment and CFD is approximately within 3% which is encouraging in that CFD simulation may be able to be a replacement of resistance and self propulsion experiments for twin-skeg ships. The results from I2 and I3 indicate that not only resistance and self propulsion coefficients

but also local flow and POC are also very well predicted by the present CFD simulation. The optimal propeller location is successfully identified by the present CFD simulation as well. In addition, the information of stern flow field estimated by the present simulation recently utilized to design twisted rudder which contributes to improve propulsive performance of a certain twin-skeg ship¹⁹⁾. The results from I4 provide thought-provoking information to come up with better scaling criteria for 1-w_T of twin-skeg ships and POC for podded propulsor. Although it is difficult to perform, full scale validation would be required to put these results into practical use. The results from I5 suggest guidelines for design of skeg geometry which can be applicable for twin-skeg ships with podded or line-shaft propulsors. The results from I6 show flexibility of unstructured grid generation as well as feasibility of the UBA by full CFD simulations.

Reference

- 1) Sasaki N., 2010, What is the best propeller for ZEUS?, Proc. International Propulsion Symposium, Okayama, Japan, pp. 116-123.
- 2) Miyazaki H., Ueno M. and Tsukada Y., 2011, Numerical study about stern skeg on course stability, Proc. The 21st International Offshore and Polar Engineering, Maui, USA, pp.964-969.
- 3) Sasaki N., 2011, Boundary layer control of twin-skeg hull form with reaction podded propulsion, Proc. The 2nd International Conference on Marine Propulsors, Hamburg, Germany, pp.244-249.
- 4) Lee YY., Lee CJ, Van SH, Hwang YS, Park JS, Kim SP and Park NJ, 2003a, A development of basic hull forms and survey on the performance for twin skeg mega container ship [in Korean], Proc. Annual Spring Meeting, The Society of Naval Architectures of Korea, pp. 24-28.
- 5) Lee YY, Lee CJ, Van SH, Park JS, Kim YS and Park NJ, 2003b, Investigation of powering performance with parametric variation of distance and vertical angle of twin skegs [in Korean], Proc. Annual Autumn Meeting, The Society of Naval Architectures of Korea.
- 6) Van SH, Park IR, Kim J, Lee YY, Park NJ and Kim YS, 2004a, Hydrodynamic performance analysis of twin skeg container ship using CFD simulation, Proc. The 4th Conference on New Ship and Marine Technology, Shanghai, China.
- 7) Van SH, Park IR, Kim J, Park NJ and Choi YB, 2004b, Hydrodynamic performance analysis for the twin-skeg container ship, Proc. The 11th Symposium of Practical Design of Ships and Other Floating Structures, Luebeck-Travemuende, Germany.
- 8) Park DW and Chun HH, 2009, Design practice for the stern hull form of a twin-skeg ship, Journal of Marine Science and Technology, Vol. 14, Issue3, pp.310-321.
- 9) Kume K and Hirata N, 2009, Flow analysis for twin-skeg type ship on locally refined unstructured hexahedral grids [in Japanese], Proc. The 23rd CFD Symposium, Sendai, Japan.
- 10) Kume K and Hirata N, 2010, Numerical simulation of a twin-skeg ship with working propellers [in Japanese], Proc. 24th CFD Symposium, Yokohama, Japan.
- 11) Ochi F and Nagaya S., 2011, Flow pattern of twin skeg hull form –PIV measurement and CFD analysis [in Japanese], Proc. Annual Autumn Meeting, The Japan Society of Naval Architects and Ocean Engineering, Tokyo, Japan.
- 12) Kawabuchi M, Kawakita C, Mizokami S, Higasa S, Kodan Y, and Takano S, 2011, CFD predictions of bubbly flow around an energy saving ship with Mitsubishi air lubrication system, Mitsubishi Heavy Industry Technical Review, Vol. 48, Issue 1, pp.53-57.
- 13) Spalart PR and Allmaras SR, 1994, A one-equation turbulence model for aerodynamic flows, La Recherche Aeronautique, Vol. 1, Issue 1, pp. 5-21.
- 14) Ohashi K, Hirata N and Hino T, 2003, A comparative study of body force models representing effects of contrarotating propellers, Proc. The 105th Meeting of the

- West-Japan Society of Naval Architects, pp.55-64.
- 15) Moriyama F, 1979, On an approximate numerical method for estimating the performance of marine propellers [in Japanese], Annual Report of Ship Research Institute, Vol. 16, Issue 5, pp. 361-376.
 - 16) Hino T, Hirata N, Miyazaki H and Ohashi K, 2008, Ship performance evaluation using CFD, Proc. The 3rd PAAMES and AMEC 2008, Chiba, Japan, pp. 89-98.
 - 17) HullDes Ver6.0 User's manual, ACT Co.,Ltd.,<http://www.actechnology.co.jp/english/index.html>
 - 18) Lackenby, H., 1950, On the systematic geometrical variation of ship forms, Transactions of the Institute of Naval Architects, vol.92, 289-316.
 - 19) Sakamoto N, Kawanami Y and Ichinose Y, 2013a, Investigations of design criteria for ships with split-stern by viscous CFD, Proc. The 13th Research Presentation Meeting of National Maritime Research Institute, pp.9-16.
 - 20) Sakamoto N, Kawanami Y, Uto S and Sasaki N, 2013b, Estimation of resistance and self-propulsion characteristics for low L/B twin-skeg container ship by a high-fidelity RANS solver, Journal of Ship Research, Vol. 57, No.1, pp.24-41.
 - 21) Sakamoto N, Kawanami Y, Ohashi K and Uto S, 2013c, RANS simulations of podded propulsor in model and full scale, Proc. Annual Spring Meeting, The Japan Society of Naval Architects and Ocean Engineering, Hiroshima, Japan.
 - 22) International Towing Tank Conference, 1978, Report of performance committee, Proc. 15th International Towing Tank Conference, Hague, Netherlands, pp.364-366.
 - 23) Sakamoto N, Kawanami Y and Uto S, 2011, Computational study for single-screw and twin-skeg container ships in full scale by unstructured grid based RANS solver, Proc. Annual Fall Meeting, The Japan Society of Naval Architects and Ocean Engineering, Tokyo, Japan.
 - 24) Sakamoto N, Kawanami Y and Uto S, 2012, Investigations of design criteria for ships with split-stern by RANS, Proc. The 15th Numerical Towing Tank Symposium, Cortona, Italy.
 - 25) Shipbuilding Research Centre of Japan, 2004, SRC News, No. 53.
 - 26) Ukon Y and Fujisawa J, 2004, Self propulsion test and its analysis method for ships with podded propulsor [in Japanese], Proc. The 4th Research Presentation Meeting of National Maritime Research Institute, Tokyo, Japan.
 - 27) Koyama K, 1972, A numerical analysis for the lifting surface theory of a marine propeller, Proc. The Society of Naval Architects of Japan Fall Meeting, pp.91-98.
 - 28) Sakamoto N, Kawanami Y, Ohashi K and Uto S, 2013d, RANS simulations of twin-skeg container ship with podded propulsor by unit-based self propulsion analysis, Proc. Annual Spring Meeting, The Japan Society of Naval Architects and Ocean Engineering, Hiroshima, Japan.